A lamellar coordination polymer with remarkable catalytic activity

Mendes, Ricardo F ; Antunes, Margarida M ; Silva, Patrícia ; Barbosa, Paula ; Figueiredo, Filipe ; Linden, Anthony ; Rocha, João ; Valente, Anabela A ; Almeida Paz, Filipe A

DOI: https://doi.org/10.1002/chem.201602157

Lamellar Coordination Polymer with a Remarkable Catalytic Activity

Ricardo F. Mendes,[a] Margarida M. Antunes,[a] Patrícia Silva,[a] Paula Barbosa,[b] Filipe Figueiredo,[b] Anthony Linden,[c] João Rocha,[a] Anabela A. Valente,[a,*] Filipe A. Almeida Paz[a,*]

A contribution from

[a]*Department of Chemistry, CICECO – Aveiro Institute of Materials, University of Aveiro, 3810-193 Aveiro, Portugal. E-mails: atav@ua.pt; filipe.paz@ua.pt*

[b]*Department of Materials & Ceramic Engineering, CICECO – Aveiro Institute of Materials, University of Aveiro, 3810-193 Aveiro, Portugal*

[c] *Department of Chemistry, University of Zürich, CH-8057 Zürich, Switzerland*

* *To whom correspondence should be addressed:*
Filipe A. Almeida Paz
Department of Chemistry, CICECO – Aveiro Institute of Materials
University of Aveiro
3810-193 Aveiro
Portugal

E-mail: filipe.paz@ua.pt
FAX: (+351) 234 401470
Telephone: (+351) 234 401418

Abstract

A new positively charged lamellar coordination polymer based on a flexible triphosphonic acid linker is reported. $[Gd(H_4nmp)(H_2O)_2]Cl{\cdot}2H_2O$ (**1**) [where H_6nmp stands for nitrilotris(methylenephosphonic acid)] is obtained in a typical one-pot approach using water as a "green" solvent and by forcing the inclusion of additional acid sites by employing HCl in the synthesis. Compound **1**performs as a heterogeneous, versatile acid catalyst, with outstanding activityin different organic reactions, namely, the alcoholysis of styrene oxide, acetalisation of benzaldehyde and ofcyclohexanaldehyde, and ketalisation of cyclohexanone. For all reaction systems, very high conversions were reached (92-97%) in only 15-30 min, under mild conditions (35 ºC, atmospheric pressure). Allied to these catalytic results, the material also exhibits interesting protonic conductivity values of $1.23x10^{-5}Scm^{-1}$ at 98% RH at 40 ºC.

Keywords: Metal-Organic Frameworks; Layered Materials; Heterogeneous Catalysis; Alcoholysis of epoxides; Acetalisation of benzaldehyde and cyclohexanaldehyde; Ketalisation of cyclohexanone; Proton conduction

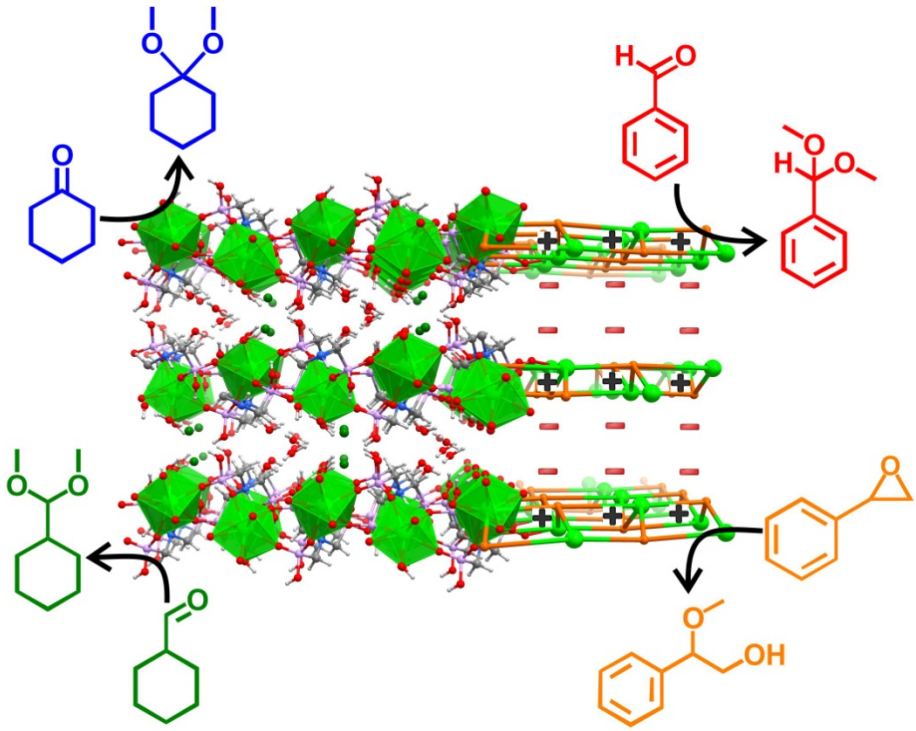

1. Introduction

Research on Metal-Organic Frameworks (MOFs), and Coordination Polymers (CPs), is currently driven by the need to employ such materials in important technological areas for society by taking advantage of the high versatility of these networks.[1] The great ability to tailor specific chemical and physical functionalities into MOFs has led to a boost of interest by industry in these materials,[2] mostly driven by the intrinsic wide diversity of applications and properties: fabrication of membranes or thin films,[3] application in biomedicine,[4] as imaging contrast agents,[5] in magnetism studies,[6] catalysis,[7] ion exchange,[8] and in proton conduction.[9] Over the last few years our research group has been focusing on the design of novel networks based on polyphosphonic acid ligands and rare-earth cations. This combination of building units, particularly the use of phosphonic chelating units, has been found to induce the formation of highly robust dense networks,[10] some of which exhibit true multifunctionality (*e.g.*, photoluminescence combined with catalytic activity).

A common feature among this type of crystalline hybrid materials, particularly the materials designed and developed in our research group, concerns the large concentration of acidic protons and solvent (typically water) molecules. We are currently looking on taking advantage of this particular structural feature in order to design better performing MOFs which take advantage of proton mobility and/or exchange. In this report we describe our most recent efforts to design and prepare the novel crystalline layered MOF $[Gd(H_4nmp)(H_2O)_2]Cl{\cdot}2H_2O$ (**1**) [where H_6nmp stands for nitrilotris(methylenephosphonic acid); see scheme S1 in the ESI] which proved, on the one hand, to be a much better and efficient heterogeneous catalyst in a wide range of reactions and, on the other, a promising proton conductor. While using the flexible nitrilotris(methylenephosphonic acid) (H_6nmp) organic linker and Gd^{3+} metallic centers, the deliberate inclusion of HCl in the reaction system forced the anchoring of additional catalytic sites in the resulting MOF, with the concomitant inclusion of charge-balancing chloride anions occupying the interlayer space. **1** has been prepared using one-pot approaches (see Experimental Section for detailed information), which is a more environmentally-friendly alternative to the traditional hydrothermal and microwave-based approaches routinely used in our group. This approach allows the preparation of a high quantity of the desired material while significantly reducing the reaction time and energy consumption (*vs.* hydrothermal approaches). Water, the most "green" solvent used in industry, was employed for the preparation of **1**, while adding a small quantity of HCl. As mentioned above, the use of HCl allowed the design of a larger concentration of acidic centers in the material with the final aim of improving the catalytic performance of the compounds. Besides influencing the chemical features of the MOF, the use of HCl also allowed the increase of the crystallite size by slowing down the deprotonation of the organic linker (thus favoring crystal growth over nucleation).

2. Results and Discussion

2.1. Structural Description

Compound **1**, formulated as$[Gd(H_4nmp)(H_2O)_2]Cl{\cdot}2H_2O$,crystallizes in the non-centrosymmetric monoclinic *I*a space group (

Table 1), being composed of infinite 2D positively charged layers, counter balanced by chloride ions which are located in the interlayer spaces.

The asymmetric unit consists of one eight-coordinated Gd^{3+} center, one bridging and chelating H_4nmp^{2-} anionic organic linker, two coordinated and two uncoordinated water molecules plus the charge-balancing uncoordinated chloride anion (Figure S1). The crystallographic single Gd^{3+} center is coordinated to a total of six phosphonate groups arising from four symmetry-related H_4nmp^{2-} anionic organic linkers and two coordination water molecules, with the $\{GdO_8\}$coordination polyhedron resembling a distorted dodecahedron (Figure 1). The Gd–O bond lengths were found in the 2.326(3)-2.564(3) Å range, which is comparable to those reported for other Gd^{3+}-based phosphonate compounds. The internal O–Gd–O polyhedral angles were found in the 65.37(11)-150.53(11)º range (Table 2). H_4nmp^{2-} acts as a hexadentate organic linker connecting four symmetry-related metal centers. All phosphonate groups act μ_2-O,O'-bridging moieties, with two of them being connected to the same pair of metal centers. As reported for the related $[Pr(H_3nmp)]{\cdot}1.5H_2O$ compound,[11] this high connectivity of the H_4nmp^{2-} organic ligand is responsible for the trapping of Gd^{3+} centers inside a phosphonic-type inorganic matrix.

The layer arrangement is composed of one-dimensional inorganic zigzag chains running parallel to the *c*-axis of the unit cell, formed by Gd^{3+}polyhedra interconnected by three phosphonate groups from two different H_4nmp^{2-} ligand residues [intermetallic Gd···Gd distance of 5.6081(3) Å]. The organic part of the ligand bridges these inorganic chains, forming a layer parallel to the *ac* plane with an additional intermetallic Gd···Gd distance of 8.4834(3) Å (Figure 2). The organic linker in **1** acts as a typical zwitterionic species, with the central nitrogen atom being protonated and the peripheral phosphonates groups being, each, singly negatively charged ($–PO_3H^-$). We note that this zwitterionic behavior has already been observed for other compounds based on aminophosphonate residues.[11-12] The protonated P–OH groups and coordinated water molecules of the $_\infty^2[Gd(H_4nmp)(H_2O)_2]^+$ cationic layer donate their hydrogen atoms to neighboring water molecules of crystallization and to the chloride anion (Table S1, Figure S2).

---Insert Figure 1---

To the best of our knowledge **1** constitutes the first example of a phosphonate-based MOF having positively charged 2D layers, balanced in the interlamellar space by uncoordinated chloride ions (Figure 2). This structural feature finds some structural resemblances with the naturally-occurring layered

double hydroxides (LDH), which are anionic clay materials with demonstrated usefulness in a wide range of applications, such as heterogeneous catalysts of a variety of organic reactions.[13] We note that for LDHs a variety of charge-balancing ions can be intercalated, ultimately improving catalytic activity. The presence of intercalated chloride anions in **1** has the same effect: two neutral layered materials based on the same organic linker and previously reported by our group, [La(H_3nmp)][10b] (isolated from microwave-assisted synthesis) and [Pr(H_3nmp)]·1.5H_2O (prepared using hydrothermal synthesis),[11] performed comparatively poorly as heterogeneous acid catalysts with respect to the results herein described for **1**. All compounds have a 2D layered structure with the difference that **1** has positively charged sheets involved in strong hydrogen-bonding interactions. Looking at the structures from a topological perspective (*i.e.*, reducing each network to central nodes and connecting bridges), one can see that they are, nevertheless, very similar: on the one hand, the three layered networks are assembled by a single crystallographic independent Ln^{3+} center; on the other, the asymmetric unit is also composed of one $H_{6-x}nmp^{-x}$ (x =3 or 4) residue. Structural differences occur, indeed, in the quantities of water molecules and the non-coordinating chloride ions for **1**. Thus, each organic residue is connected to four crystallographically independent Ln^{3+} centers, with all compounds being topologically uninodal networks with 4-connected nodes and Schläfli point symbols of $\{4^4.6^2\}$ (Figure 2and Figure S3 in ESI).

---Insert Figure 2---

Structural differences between **1** and [La(H_3nmp)] or [Pr(H_3nmp)]·1.5H_2O arise, mainly, from the supramolecular interactions present between the layers. In **1**, coordinated water molecules and protonated P–OH groups interact with charge-balancing chloride anions and water molecules of crystallization, ultimately leading to a stronger close packing of cationic layers. In [Pr(H_3nmp)]·1.5H_2O, which is also a hydrated material, the supramolecular interactions are limited to hydrogen bonds between P–OH groups and crystallization water molecules. These interactions are, thus, weaker than those found in **1**, resulting in a higher thermal stability for the latter: while in [Pr(H_3nmp)]·1.5H_2O the water molecules of crystallization are completely removed at *ca.* 75 ºC immediately accompanied by a structural modification, **1** is stable up to *ca.* 150 ºC. For [La(H_3nmp)] the interaction between layers is notably different: without solvent molecules the interaction between layers is achieved mainly by hydrogen bonding interactions associated with the protonated P–OH groups. Although the connectivity is the same for all three compounds, in the case of [La(H_3nmp)] four metal centers are connected by a single phosphonate group forming a far more compact layer.

2.2. Thermoanalytical and Vibrational Studies

The level of hydration level observed in the crystal structure was investigated by thermogravimetric analysis between ambient temperature and *ca*. 800 ºC (Figure 3). The bulk $[Gd(H_4nmp)(H_2O)_2]Cl{\cdot}2H_2O$ (**1**) show a consecutive weight loss with no visible plateaus. Nevertheless, as seen in Figure S1 one can divide the thermogram into three main regions, each corresponding to a combined weight loss. The first region, located between ambient temperature and *ca.* 195 ºC, is attributed to the release of four water molecules (two of crystallization and two of coordination), corresponding to a total weight loss of 12.6% (calculated 12.8%). When the temperature is increased the material undergoes a crystalline phase transition, as clearly observed from the performed variable-temperature powder X-ray diffraction studies. There is some peak broadening (suggesting loss of crystallinity) and reflection dislocations, which is an indication of variation of the unit cell dimensions. We note that these structural modifications may suggest a closer proximity between the gadolinium oxide layers within the temperature-modified structure, a feature observed for $[La(H_3nmp)]$.[14]

The next weight loss, in the range of about 195-355 ºC (4.4%), can be attributed to the partial release of a hydrochloric acid residue (calculated 6.5%). The difference in calculated and observed weight loss might be due to the presence of agglomerates in the sample leading to an entrapment of the hydrochloric acid, which will be ultimately released at higher a temperature. To corroborate this assumption we have performed EDS analysis of the material calcined at different temperatures, clearly showing that up to *ca*. 350 ºC all the chloride anions are released from the material (Figure 3 – inset; Figures S5 and S6 in the ESI). Noteworthy, the release of HCl is accompanied by an overall loss of crystallinity.

Above *ca.* 350 ºC additional weight losses (6.1% and 5.6% in the ranges of about 350-550 ºC and 550-800 ºC, respectively) are attributed to the full decomposition of the organic component. The residue reminiscent at *ca*. 800 ºC agrees well with the stoichiometric formation of the inorganic residue GdO_9P_3 (PDF4+ database, release 2012, reference code 04-015-0835).

The vibrational spectrum (Figure S7 in ESI) contains a series of bands centered at about 3400 cm^{-1} attributed to the υ(O–H) stretching vibrational modes from both coordination and crystallization water molecules. The typical symmetric and asymmetric υ(C–H) and υ(N–H) stretching vibrational modes appear in the 3100-2750 cm^{-1}spectral region. The latter mode is found at about 3057 cm^{-1}, while the signals peaking at about 3027, 2982, 2954 and 2778 cm^{-1} are attributed to the $\upsilon_{sym+asym}$(C–H) vibrational modes. In the central spectral region, between 1500 and 1300 cm^{-1}, a number of very weak bands can be attributed to υ(C–H) modes characteristic of P–CH_2 groups. The typical P–OH stretching modes were also observed between 2200 and 2400 cm^{-1} as faint and broad bands. In the range of 1500-600 cm^{-1} it is possible to discern the typical υ(C–N) stretching vibrational modes of tertiary amines assigned to the intense bands peaking at about 1133, 1096 and 1075 cm^{-1}. The υ(P–C) stretching vibrational modes are also observed, in particular between *ca*. 790-690 cm^{-1}. Also in this region, the stretching vibrational

modes of υ(P=O) are clearly noticed between *ca*. 1340 and 1145 cm^{-1}, plus those of υ(P–O) between *ca*. 1040 and 860 cm^{-1}.

---Insert Figure 3---

2.3. Heterogeneous catalysis

$[Gd(H_4nmp)(H_2O)_2]Cl{\cdot}2H_2O$ (**1**) was tested as a heterogeneous catalyst for various important acid-catalysed reactions in both academia and chemical industry: epoxide alcoholysis, acetalisation of aromatic and aliphatic aldehydes, and ketalisation of ketones. Epoxide ring opening reactions can afford β-alkoxy alcohols, which are functional, versatile intermediates used in (in)organic syntheses.[15] On the other hand, acetalisation/ketalisation reactions are important transformations in organic chemistry enabling the protection of carbonyl groups in the presence of other functional/reactive groups.[16]Acetal and ketal chemicals can advantageously possess high stability under basic conditions, and are stable to Grignard reagents, metal hydrides, oxidants, halogenation, and esterification reagents.[17] Ketals and acetals are used in the production of perfumes, fragrances and flavours,[18] cosmetics, in the food and beverage industries,[18-19] in pharmaceuticals,[18a, 18b, 20] plasticizers,[21] solvents and other intermediates.[18a, 18c, 22] Homogeneous mineral acids (HCl, H_3PO_4 and H_2SO_4) and metal triflates[23] are generally used in these reactions.[24] Nevertheless, these chemical reactions can be more environmentally friendly and economically feasible if one uses more efficient heterogeneous catalysts. Compound **1** possesses a remarkable catalytic activity for these various chemical reactions, studied under atmospheric conditions while using relatively cheap alcohols as reacting solvents (methanol or ethanol). We direct the reader to Tables S2, S3 and S5 (in the Electronic Supporting Information) for a comparative analysis of the catalytic performance of **1** and of various MOFs reported in the literature. The various parameters that influence the catalytic reactions are generally different between studies, making it difficult to make rigorous, fair comparisons. Whenever possible, the catalytic results for**1**in each reaction system are compared to literature data in the following discussion.

---Insert Figure 4---

Styrene oxide alcoholysis

These tests were performed with methanol and ethanol, always giving the corresponding β-alkoxy alcohol product with 100% selectivity, and excellent yields, under approximately atmospheric conditions (35 ºC, atmospheric air). Methoxy-2-phenylethanol was obtained with 97% yield after only 30 min reaction of styrene oxide with methanol, and 2-ethoxy-2-phenylethanol was obtained with 100% yield after4h of reaction when ethanol was used instead (Figure 4).

In order to gain insights into the type of acidity, the catalytic performanceof**1**was compared to that of the ligand(H_6nmp) and the lanthanide (Gd_2O_3) precursors. H_6nmp produced 2-methoxy-2-phenylethanol as the sole product formed with 97% yield at 30 min. The lanthanide precursor led, on the other hand, to a negligible styrene oxide conversion at 4 h (Figure S8). The catalytic activity of **1** resembles more closely that of the ligand precursor than of the lanthanide one, suggesting that the high catalytic activity of **1**is due to Brönsted acid sites, which may be associated with its organic component. The Brönsted acidity associated with the P–OH groups in **1** can favour the protonation of the oxygen atom of the epoxide group. This leads to a favourable nucleophilic attack of the alcohol reagent at the more substituted carbon atom of the epoxide group, leading to the corresponding β-alkoxy alcohol product. A possible reaction mechanism is hypothesized in (in the ESI). Even though H_6nmp is an effective organocatalyst, the catalytic process is homogeneous in nature with implications in terms of demanding catalyst separation/regeneration.

Compound **1** was re-used in three consecutive reactions showing no considerable change in the conversion rate and maintaining its structural integrity (Figure 5and Figure S10 in the ESI).The heterogeneous nature of catalyst **1** was assessed by a leaching test at 35 ºC. After separating the solid catalyst from the reaction mixture at 15 min the conversion of styrene oxide ceased to increase (remaining at *ca.* 15%), which is an indication of the absence of soluble active species (Figure S9 in the ESI).For comparison, the reaction of styrene oxide was carried out using HCl as homogeneous catalyst (in an amount equivalent to that of Cl added with the MOF in a normal catalytic test), giving the β-alkoxy alcohol product with 97% yield at 15 min. As a consequence, if the solution of the leaching test for **1**contained any HCl, conversion should have increased, which was not observed.

---Insert Figure 5---

The catalytic activity of **1** is comparable or superior to that of the 1D MOFs $[La_2(H_3nmp)_2(H_2O)_4]\cdot 4.5H_2O$[25] and $[La(H_4bmt)(H_5bmt)(H_2O)_2]\cdot 3H_2O$[26] previously reported by our groups (100% conversion after 3 and 6 h reaction, respectively)(Table S2 in ESI).Although**1** is based on the same ligand as $[La_2(H_3nmp)_2(H_2O)_4]\cdot 4.5H_2O$,[25] it possesses instead a 2D layered structure with electron-withdrawing chloride ions located in the interlamellar space. Vermoortele *et al.*[27]reported that electron-withdrawing groups, such as nitro groups in UIO-66Zr-NO_2,may influence the acid properties and induce (de)stabilizing effects on transition states, enhancing the catalytic activity. The positive effect of NO_2 groups on catalytic activity when compared to the original MOF tested was found for various reactions, namely the cyclisation of (+)-citronellal, conversion of geraniol,[27] and reduction of 4-tert-butylcyclohexanone.[28] In this way, we envisage that the electron-withdrawing chloride anions between the layers of **1** account for the enhanced catalytic activity. The activity of **1** is slightly surpassed by a MOF-supported heteropolyacid, namelyMIL-101(HPW) (99% conversion and 99% selectivity at

0.33 h and 40 ºC).[29] The synthetic procedure of this latter MOF is, however, much more complex, requiring higher temperatures, the need to synthesize the heteropolyacid, and activation under vacuum at 140 ºC. In addition it suffered partial loss of catalytic activity over several cycles.

Acetalisation of benzaldehyde

In this reaction 100% selectivity towards the benzaldehyde dialkylacetal product with excellent yields was observed: 92% benzaldehyde dimethyl acetal yield after 1h, and 56% benzaldehyde diethyl acetal yield after 6 h, for the reaction with methanol and ethanol, respectively (Figure 4). A possible mechanism of the Brönsted acid-catalysed alcoholysis of benzaldehyde is depicted in Scheme S3 (in the ESI).[30]A Brönsted acid site protonates the oxygen atom of the carbonyl group leading to the intermediate formation of a hemiacetal which, after water elimination, gives a carbocation. The latter undergoes a nucleophilic attack from another alcohol molecule giving the acetal product. The hemiacetal intermediate was not detected possibly due to its high reactivity under the catalytic conditions used.

The catalytic results for **1**are far superior to those previously reported for the 1D MOF $[La_2(H_3nmp)_2(H_2O)_4]\cdot 4.5H_2O$ tested under identical reaction conditions (94% benzaldehyde dimethyl acetal yield after 20 h using a catalyst load of20 g L^{-1}) (Table S3 in ESI),[25] which may be partly related to the electron-withdrawing effects reported by Vermoortele *et al.* (and as discussed above).[27] The catalytic activity of **1** is, in this context, one of the best reported to date, surpassing those of $[Al_2(BDC)_3]$, [Fe(BTC)], $[Cu_3(BTC)_2]$, MIL-100(Fe) and UIO-66 (Table S3 in the ESI).[31] Compound**1** performed similarlyto MIL-101(PTA)[32], MIL-101-NO_2d[30] and UIO-66-NO_2[33] which required, nevertheless, a thermal activation prior to use, whereas no pre-treatment was applied to the material herein reported.

Ketalisation of cyclohexanone

Reactions were performed with methanol or ethanol at 35 and 55 ºC. With methanol, 93% cyclohexanone conversion was reached after 15 min (35 ºC) (Figure 4) or after 5 min (55 ºC), with the main reaction product being cyclohexanone dimethyl ketal (*ca.* 92-94% selectivity at *ca.* 93% conversion). Methoxycyclohexene was formed as a by-product (*ca.* 6-8% selectivity, Table S4 in the ESI). With ethanol, the corresponding ketal was formed with 94% selectivity at 81% conversion after 15 min (35 ºC). Ethoxycyclohexene was also observed as a by-product (*ca.* 3% selectivity, Table S4 in the ESI). The mechanism of the Brönsted acid-catalysed ketalisation reaction in alcohol media may be similar to that of the acetalisation of benzaldehyde and is presented in Scheme S4 in ESI.

Only two other previously investigated MOFs in the ketalisation of cyclohexanone are known, namely $[Cu_3(BTC)_2]$[31a] and MIL-101-Cr-NO_2d.[30] $[Cu_3(BTC)_2]$ was less active than **1** (80% conversion at 24 h), and the catalytic results forMIL-101-Cr-NO_2dare roughly comparable to those for **1** (90% conversion at 1.5 h using slightly less amounts of catalyst and substrate at 25 ºC). The catalytic

performance of **1** compares favourably to other solid acids, such as zeolites (H-Y,[34] H-ZSM5,[35] H-Mordenite,[35d] H-beta,[35c, 35d] mesoporous aluminosilicates Al-MCM-41[35c, 36]) and heteropolyacid-based catalysts (*e.g.*, $H_3PW_{12}O_{40}$)[35c] (see Table S5 in the ESI for further details). Sulfonated metal oxides led to 100% conversion of cyclohexanone after 30 min under similar reaction conditions (*e.g.*, SO_4^{2-}/ZrO_2, SO_4^{2-}/TiO_2, SO_4^{-2}/SnO_2[37]), albeit tetramethylorthoformate was used as aketalisation agent and tetrachloromethaneas the solvent, whereas in the present work, a relatively inexpensive alcohol with the dual function of reagent-solvent was used.

Acetalisation of cyclohexanaldehyde

Cyclohexanaldehyde was reacted with methanol or ethanol at 35 ºC or 55 ºC. With methanol, **1** led to (dimethoxymethyl)cyclohexane in 88% yield at 93% conversion after 1 h (35 ºC) (Figure 4). Identified by-products included cyclohexane carboxylic acid and methyl cyclohexanecarboxylate (Table S6 in the ESI). The reaction with ethanol led to 86% yield of (diethoxymethyl)cyclohexane at 90% conversion, 1 h (35 ºC), with by-products including ethylcyclohexanecarboxylate (Table S6 in the ESI). The use of methanol and an increase of the reaction temperature to 55 ºC under autogeneous pressure, led to methylcyclohexanecarboxylate as the sole observed product in 76% yield after 1 h. The mechanism for this reaction is also similar to the acetalisation of benzaldehyde (Scheme S5 in the ESI). The hemiacetal was identified by GC-MS for the reaction with ethanol. To the best of our knowledge, catalyst **1** constitutes the first example of a MOF being investigated for the acetalisation of cyclohexanaldehyde in acidic medium. Clerici*et al*.[38] reported the acetalisation of cyclohexanaldehyde with MeOHin the presence of $TiCl_4$ in basic medium, which led to 94-98% acetal yield at 30 min and 0 ºC. Although this constitutes a rather interesting result, when compared to **1**, that reaction system was significantly more complex comprising the use of relatively toxic bases such as NH_3 or trimethylamine and the need for a refrigeration system to maintain low temperatures.

General considerations

The conversion versus times curves for the acetalisation and ketalisation reactions reached a plateau after *ca.* 2 h reaction due to thermodynamic limitations caused by the presence of water, formed as a co-product of the catalytic reaction. Similar kinetics effects were reported by Arrozi *et al.* for UiO-67 tested in benzaldehyde acetalisation.[31c]Considerable differences in reaction rates were observed for **1** when ethanol of PA quality was used instead of anhydrous ethanol: with anhydrous ethanol, benzaldehyde diethylacetal yield at 6 h was 56%, whereas with ethanol PA, the yield was 23%.Ren *et al.*[39] also reported that the reaction of benzaldehyde with methanol in the presence of the 3D MOF $[Tb_2(dpa)_3]$ (H_2dpa=1,4-phenylenediacetic acid) was considerably affected by water. When stoichiometric amounts of water were initially added to the reactor, conversion at 10 h and ambient temperature was 22%, compared to 78% conversion without the addition of water. On the other hand,

Garcia *et al.*[40] reported for (2D) $[(K\text{-}18\text{-}crown\text{-}6)_3][M_3^{II}(H_2O)_4(Ru(ox)_3)_3]$ (M=Cu, Co, Fe, Mn and Zr; ox=$C_2O_4^{2-}$) that the benzaldehyde dimethyl acetal yields could be slightly improved (from 50-83% to 56-98%, at 24 h/70 ºC) after applying a thermal/vacuum pre-treatment to the MOF.

The reaction tended to be faster with methanol than with ethanol. These results agree with literature data for other MOFs tested as catalysts in the same reaction,[10b, 25, 41] and may partly be due to steric hindrance effects. In all tested catalytic reactions a six-fold decrease in the amount of **1** from 20 to 3.3 g_1 L^{-1} (and methanol as solvent) led to similar outstanding catalytic results. The catalyst could easily be recovered by washing/drying, and maintained its structural integrity after 3 runs for the styrene oxide alcoholysis (Figure 5 and Figure S10 in the ESI) and after the acetalisation of benzaldehyde, the ketalisation of cyclohexanone and acetalisation of cyclohexanaldehyde(Figure S11 in the ESI).

2.4. Proton Conduction

The mechanism of ion conduction in a solid material is mainly influenced by its structure, temperature and by the amount and mobility of charge carriers. The presence of phosphonate-containing ligands with hydrogen-bonded chains makes $[Gd(H_4nmp)(H_2O)_2]Cl{\cdot}2H_2O$ (**1**) a suitable host structure to enable ionic transport along interlayer channels, where the adsorption of water molecules facilitated by the phosphonic acid groups provides paths for the structural diffusion of protons. Compound **1** was processed into pellets in order to be used for the electrical measurements. These could easily be obtained free from major defects from the starting material, while preserving crystallinity. For this study, two pellets were prepared: one used immediately after processing (**1p**), while the other was left at 120 ºC overnight (**1p_dry**).

Figure S12 (in the ESI) shows impedance spectra obtained for these two samples at 40 ºC highlighting the effect of relative humidity (RH) on their shape and on the relaxation frequency of the relevant phenomena contributing to the impedance. The plots for RH lower than 80% depict a single, slightly depressed semicircle with amplitude corresponding to the bulk resistance of the sample, which was used to obtain the conductivity. The amplitude of the semicircle decreases substantially with increasing humidity, and the shape changes substantially for 98% RH. In these nearly saturated humidity conditions, the **1p_dry** spectrum depicts a well-defined semicircle at high frequency, plus a depressed semicircle at intermediate frequencies, which dominates the total impedance and is strongly overlapping with a capacitive tail at low frequency. The two contributions at high frequency are ill-defined in the **1p** spectrum, which appear as one single, highly depressed semi-circle in series with a (in this case) clearly separated low frequency tail. The latter may be ascribed to the electrode impedance, whereas the high and intermediate frequency contributions are due to the impedance of the pellets. The comparison of the distribution of relaxation frequencies for **1p** and **1p_dry** further suggests that the intermediate frequency

semicircle is strongly dependent on the hydration of the sample, being smaller for **1p**. The materials maintain their structure and their crystallinity after these measurements.

The conductivity of **1p** and **1p_dry** at 40 ºC, plotted as a function of RH in Figure 6, increases by approximately five orders of magnitude with increasing RH from 20 to 98%, indeed suggesting proton transport. The conductivity of **1p** is higher than **1p_dry**, but the differences tend to decrease with increasing RH. This may indicate an increasing contribution of proton transport through water molecules adsorbed on the surface of the MOF particles with increasing RH, whereas bulk transport should predominate for low RH. The maximum measured conductivities (at 40 °C and 98% RH) are 1.23×10^{-5} $Scm^{-1}$and 3.49×10^{-6} Scm^{-1} for **1p** and **1p_dry**, respectively. These values are comparable to various other non-porous phosphonate MOFs and CPs with similar water content.[42]

---Insert Figure 6---

3. Conclusion

In summary, we report the sustainable preparation of a cationic lamellar coordination polymer obtained by the self-assembly of Gd^{3+} and a polyphosphonic acid linker. Though the structure shares similar features to previously reported layered materials obtained by our group, the structural design of positively charged layers was managed using HCl in the synthesis. This led to the isolation of a new material which is a heterogeneous and versatile catalyst, exhibiting remarkable activity in four different reactions: alcoholysis of styrene oxide, acetalisation of benzaldehyde, ketalisation of cyclohexanone and, tested for the first time, in the acetalisation reaction of cyclohexanaldehyde. For all reactions, the reported material surpassed or, at least, equalled the catalytic results reported for other related materials studied in the literature (comprising a wide range of compounds from MOF structures to zeo-type materials).

Besides Brönsted acid properties, this new material possesses interesting proton conduction properties. At near ambient temperature and high relative humidity, the measured conductivities of the as-prepared material reaches 1.23×10^{-5} Scm^{-1}, which compares favourably with other MOFs reported in the literature.

We are currently investigating how to process these remarkable catalytic hybrid materials into functional devices (*e.g.*, as thin films or membranes) while at the same time improving other functionalities such as proton conduction and photoluminescence.

4. Experimental

4.1. General Instrumentation

SEM (Scanning Electron Microscopy) images were acquired using either a Hitachi S4100 field emission gun tungsten filament instrument working at 25 kV, or a high-resolution Hitachi SU-70 working

at 4 kV. Samples were prepared by deposition on aluminum sample holders followed by carbon coating using an Emitech K950X carbon evaporator. EDS (Energy Dispersive X-ray Spectroscopy) data and SEM mapping images were recorded using the latter microscope working at 15 kV while employing either a Bruker Quantax 400 or a Sprit 1.9 EDS microanalysis system.

Thermogravimetric analyses (TGA) were carried out using a Shimadzu TGA 50, from ambient temperature to *ca*. 800 ºC (heating rate of 5 ºC/min) under a continuous stream of air at a flow rate of 20 mL min^{-1}.

Fourier Transform Infrared (FT-IR) spectra in the range 4000-350 cm^{-1} were recorded as KBr pellets (2 mg of sample were mixed in a mortar with 200 mg of KBr) using a Bruker Tensor 27 spectrometer by averaging 256 scans at a maximum resolution of 2 cm^{-1}.

Elemental analyses for C, N and H were performed with a Truspec Micro CHNS 630-200-200 elemental analyzer at the Department of Chemistry, University of Aveiro. Analysis parameters: sample amount between 1 and 2 mg; combustion furnace temperature = 1075 ºC; after burner temperature = 850 ºC. Detection method: carbon - infrared absorption; hydrogen - infrared absorption; nitrogen – infrared absorption. Analysis time = 4 minutes. Gases required: carrier – helium; combustion – oxygen; pneumatic – compressed air.

Routine Powder X-Ray Diffraction (PXRD) data for all prepared materials were collected at ambient temperature on a Empyrean PANalytical diffractometer (Cu $K_{a1,2}$ X-radiation, λ_1 = 1.540598 Å; λ_2 = 1.544426 Å), equipped with an PIXcel 1D detector and a flat-plate sample holder in a Bragg-Brentano para-focusing optics configuration (45 kV, 40 mA). Intensity data were collected by the step-counting method (step 0.01º), in continuous mode, in the *ca*. $3.5 \leq 2\theta \leq 50^{\circ}$ range.

Variable-temperature powder X-ray diffraction data were collected on an PANalyticalX'Pert Powder diffractometer Cu $K_{a1,2}$ X-radiation (λ_1 = 1.540598 Å; λ_2 = 1.544426 Å), equipped with an PIXcel 1D detector, and a flat-plate sample holder in a Bragg–Brentano para-focusing optics configuration (40 kV, 50 mA), and a high-temperature Anton Paar HKL 16 chamber controlled by an Anton Paar 100 TCU unit. Intensity data were collected in the continuous mode (*ca.* 100 seconds data acquisition) in the angular range *ca.* $3.5 \leq 2\theta^{\circ} \leq 50$ (step 0.01º).

4.2. Reagents

Chemicals were readily available from commercial sources and were used as received without further purification: gadolinium(III) oxide (at least 99.99%, Jinan Henghua Sci. & Tec. Co. Ltd); nitrilotris(methylenephosphonic acid) [H_6nmp, $N(CH_2PO_3H_2)_3$, 97%, Fluka]; hydrochloric acid (HCl, 37% Analytical Reagent Grade, Fisher Chemical); ethanol absolute (Scharlau ACS, > 99.9%, analytical grade); ethanol absolute anhydrous (Carlo Erba, ≥ 99.9%); cyclohexanone (Aldrich, 99.8%); cyclohexanaldehyde (Aldrich, 98%); styrene oxide (Fluka, purum ≥97%); methanol (Sigma-Aldrich, chromasolv for HPLC, ≥ 99.9%); benzaldehyde (Sigma-Aldrich, 99%).

4.3. Preparation of $[Gd(H_4nmp)(H_2O)_2]Cl{\cdot}2H_2O$ (1)

A mixture containing H_6nmp (0.1425 g, 0.477 mmol) and Gd_2O_3 (0.1587 g, 0.438 mmol) in *ca.* 10.0 mL of distilled water and 10.0 mL of HCl 6 M was stirred thoroughly in a round bottom flask. The resulting solution was kept immersed at 120 ºC for 18h in an oil bath, after which time the vessel was allowed to cool slowly to ambient temperature. Crystals of $[Gd(H_4nmp)(H_2O)_2]Cl{\cdot}2H_2O$ (**1**) were readily obtained after *ca*. 15 min, and a few days later individual crystals could be harvested manually from the vessels and their structure investigated using single-crystal X-ray diffraction (see Section 4.6 for further details on the crystal selection procedures).

Elemental composition. Calculated (in %) for $[Gd(H_4nmp)(H_2O)_2]Cl{\cdot}2H_2O$ (MW = 561.80 g/mol): C 6.41, H 3.23, N 2.49.Found: C 6.40, H 3.22, N 2.34.

Selected FT-IR data (in cm^{-1}): $\nu(H_2O)_{coord}$ = 3529*w*; $\nu(H_2O)_{cryst}$ = 3447*w* and 3376*w*; ν(N–H) and $\nu_{sym+asym}$(C–H) = 3052-2981*w*; ν(POH) = 2359-2341*w*; $\delta(H_2O)$ = 1615*w*; $\delta(P{-}CH_2)$ = 1446-1401*m*; ν(P=O) = 1345-1163*m*-*vs*; $\nu[(CH_2)_3{-}N]$ = 1130-1000*vs*; ν(P−C) = 767*m* and 710*m*.

Thermogravimetric analysis (TGA) data (weight losses in %) and derivative thermogravimetric peaks (DTG; in italics inside the parentheses): 22-140ºC -9.2% (*81ºC*), 140-195ºC -3.1% (*164ºC*), 195-355ºC -4.7% (*245ºC*), 355-510ºC -6.2% (*418ºC*), 510-700ºC -4.2% (*585ºC*) and 700-800ºC -1.5%.

4.4. Catalysis

A 5 mL borosilicate batch reactor, equipped with a magnetic stirrer (800 rpm) and a valve for sampling, was charged with 1.5 mL of methanol or ethanol, 0.4 M of substrate and the solid catalyst. Substrates studied were styrene oxide, benzaldehyde, cyclohexanone or cyclohexanaldehyde. The catalytic performance of $[Gd(H_4nmp)(H_2O)_2]Cl{\cdot}2H_2O]$ (**1**) (3.3-20 $g_{\mathbf{1}}$ L^{-1}) was compared to that of the ligand and the gadolinium precursor, $H_6nmp(NC_3(PO_3H_2)_3)$ and Gd_2O_3, respectively (5.9mM, which corresponds to an equivalent molar amount of ligand or Gd^{3+} to that present in a MOF load of 3.3$g_{\mathbf{1}}$ L^{-1}). Reactions were carried out under atmospheric air, with the batch reactors immersed in an external

thermostated oil bath (35 or 55 ºC). Prior to reuse, the solid catalyst was separated from the reaction mixture by centrifugation (3500 rpm), washed with methanol or ethanol and dried under atmospheric conditions.

A leaching test was carried out for **1** by heating a stirred suspension of the MOF (3.3 $g_{\mathbf{1}}$ L^{-1}) in methanol and styrene oxide (0.4 M) for 15 min at 35 ºC, and subsequently separating the solid by centrifugation and passing the solution through a 0.20 μm PVDF w/ GMF Whatman membrane. The obtained filtrate was transferred to a pre-heated (35 ºC) batch reactor, and left to react at the same temperature under stirring.

The progress of the catalytic reactions of styrene oxide and benzaldehyde were monitored using a Varian 3800 GC equipped with a capillary column (Chrompack, CP-SIL 5 CB, 50 m x 0.32 mm x 0.5 mm) and a flame ionization detector. H_2 was usedas the carrier gas. The progress of the catalytic reactions of cyclohexanaldehyde and cyclohexanone was monitored using a GC-MS [Trace GC 2000 Series (Thermo Quest CE Instruments) - DSQ II (Thermo Scientific)] using He gas as the carrier gas.The same instrument was used for the identification of the reaction products for all substrates using the commercial databases Wiley 6 and US National Institute of Science and Technology (NIST)-Mainlib and Replib. The MS data for cyclohexanaldehyde and cyclohexanone and the corresponding acetal and ketal, respectively, are as follows:

Cyclohexanaldehyde GC-MS *m/z* (relative intensity): 112 (M^+, 18), 97 (7), 94 (57), 84 (9), 83 (95), 81 (14), 79 (30), 77 (5), 71 (8), 70 (30), 69 (6), 68 (46), 67 (12), 66 (5), 57 (9), 56 (10), 55 (100), 53 (7), 41 (22), 39 (9).

DimethoxymethylcyclohexaneGC-MS *m/z*(relative intensity): 127 (30), 95 (40), 76 (7), 75 (100), 67 (6), 47 (8), 45 (6).

DiethoxymethylcyclohexaneGC-MS *m/z* (relative intensity): 141 (30), 104 (6), 103 (100), 95 (29), 75 (26), 55 (5), 47 (15).

CyclohexanoneGC-MS *m/z* (relative intensity): 99 (M^+, 6), 98 (100), 83 (18), 80 (9), 70 (32), 69 (52), 56 (10), 55 (95), 43 (6), 42 (33), 41 (17), 39 (11).

Cyclohexanone dimethyl ketalGC-MS*m/z* (relative intensity): 144 (M^+, 11), 113 (62), 111 (6), 102 (7), 101 (100), 97 (5), 88, (7), 81 (28), 79 (6), 55 (8).

Cyclohexanone diethyl ketal GC-MS (*m/z*): 172 (M^+, 17), 130 (6), 129 (90), 127 (100), 101 (32), 99 (46), 98 (11), 97 (9), 83 (7), 81 (38), 73 (29), 70 (8), 69 (5), 55 (11).

4.5. Proton conduction

Proton conductivity (σ) of pelletized samples was studied by electrochemical impedance spectroscopy. Disc shaped samples were obtained after pressing the powders in a uniaxial press at 6.25 MPa, and then isostatically at 200 MPa. The apparent density of these pellets was obtained from

measurements of their weight and the geometric dimensions. Silver electrodes were applied on both sides of the pellets by painting with a commercial paste (Agar Scientific). Samples were placed in ceramic tubular sample holders inside a climatic chamber (ACS DY110) in order to carry out the measurements under variable temperature (40 and 60 °C) and relative humidity (RH, 20-98%). Before the measurements, one of the pellets was pre-treated overnight at 120 °C. Impedance spectra were collected between 20 Hz and 2 MHz with a test signal amplitude of 100 mV using an Agilent E4980A LCR meter. Spectra were analyzed with ZView (Version 2.6b, 1990–2002, Scribner Associates) to assess the ohmic resistance (R), which was normalized to the geometry of the samples to calculate the conductivity using the formula $\sigma = L(RA)^{-1}$, where L is the thickness of the pellets and A is the surface area of the electrodes.

4.6. Structural Determination Using Single Crystal X-ray Diffraction

One-pot synthesis allowed the preparation of several plate-like crystals that were inspected and isolated using a Stemi 2000 stereomicroscope equipped with a Carl Zeiss lenses. This allowed the identification of a large colourless plate (dimensions of about 0.05×0.2×0.27 mm) which was investigated using single-crystal X-ray diffraction. This crystal was selected manually and harvested from the batch powder and mounted in a glass fiber. Preliminary X-ray diffraction data were collected at 160(2) K on an Oxford Diffraction SuperNova, dual radiation diffractometer using a Mo Kα microsource tube (λ = 0.71073 Å), an Atlas CCDdetector, and an Oxford Instruments CryostremXL Series low temperature device.

The crystal structure of $[Gd(H_4nmp)(H_2O)_2]Cl{\cdot}2H_2O$ (**1**) was solved using the direct space algorithm implemented in SHELXT-2014,[43] which allowed the immediate location of almost all of the heaviest atoms composing the molecular unit. The remaining missing non-hydrogen atoms were located from difference Fourier maps calculated from successive full-matrix least-squares refinement cycles on F^2 using the latest SHELXL from the 2014 release.[44]

Hydrogen atoms bound to carbon, nitrogen and to the POH groups were placed at their idealized positions using appropriate *AFIX* instructions in SHELXL-2014: *147* for the hydroxy groups (identified using a combination of the chemical environment and the P–O distances), *23* for the $–CH_2–$ moieties, and *13* for the central protonated N–H group. All hydrogen atoms were included in subsequent refinement cycles with isotropic displacement parameters (U_{iso}) fixed at 1.5 (for the hydroxy hydrogen atoms) or $1.2\times U_{eq}$(for the other hydrogen atoms) of the parent atoms. Hydrogen atoms associated with the water molecules, both of crystallization and coordinated to Gd^{3+}, were directly located from difference Fourier maps and included in the structural model with the O–H and H···H distances restrained to 0.95(1) and 1.55(1) Å, respectively. This procedure ensures that these moieties refine using chemically reasonable environments. These hydrogen atoms were further included in the final structural model with the U_{iso} values fixed at $1.5\times U_{eq}$of the parent oxygen atoms.

All structural refinements were performed using the graphical interface ShelXle.[45] Structural drawings have been created using the software package Crystal Impact Diamond.[46] Information concerning crystallographic data collection and structure refinement details is summarized in Table 1. Tables 2 and S1 gather the most significant geometrical parameters of the crystallographically independent Gd^{3+} coordination sphere.

CCDC-1448427 contains the supplementary crystallographic data for this paper. The data can be obtained free of charge from The Cambridge Crystallographic Data Centre via www.ccdc.cam.ac.uk/getstructures.

ELECTRONIC SUPPORTING INFORMATION

Structural characterization details for compound **1**, including single-crystal X-ray diffraction studies, crystal structure data in CIF format, crystal structure validation, Electron Microscopy (EDS and SEM) and additional proton conductivity data. Additional data on the performed heterogeneous catalytic studies and tabulated data for related MOFs tested in the same reactions reported in the manuscript are also providedfrom the Wiley Online Library or from the author.

ACKNOWLEDGEMENTS

Funding agencies and projects

We wish to thank Fundação para a Ciência e a Tecnologia (FCT, Portugal), the European Union, QREN, FEDER through *Programa Operacional Factores de Competitividade* (COMPETE), and CICECO-Aveiro Institute of Materials, POCI-01-0145-FEDER-007679 (FCT Ref. UID/CTM/50011/2013), financed by national funds through the FCT/MEC and when appropriate co-financed by FEDER under the PT2020 Partnership Agreement. We also thank FCT for funding the R&D project FCOMP-01-0124-FEDER-041282 (Ref. FCT EXPL/CTM-NAN/0013/2013).

Individual grants and scholarships

FCT is also gratefully acknowledged for the Ph.D. grants Nos. SFRH/BD/84231/2012 and SFRH/BD/46601/2008 (to RFM and PS, respectively), the post-doctoral grants Nos. SFRH/BPD/89068/2012 and SFRH/BPD/96665/2013 (to MMA and PB, respectively), and the Development grant No. IF/01174/2013 (to FF).

References

[1] (a) M. Eddaoudi, D. F. Sava, J. F. Eubank, K. Adil, V. Guillerm, *Chem. Soc. Rev.* **2015**, *44*, 228-249; (b) M. F. de Lange, K. Verouden, T. J. H. Vlugt, J. Gascon, F. Kapteijn, *Chem. Rev.* **2015**,

115, 12205-12250; (c) A. H. Chughtai, N. Ahmad, H. A. Younus, A. Laypkov, F. Verpoort, *Chem. Soc. Rev.* **2015**, *44*, 6804-6849.

[2] P. Silva, S. M. F. Vilela, J. P. C. Tomé, F. A. Almeida Paz, *Chem. Soc. Rev.* **2015**, *44*, 6774-6803.

[3] (a) J. Gascon, F. Kapteijn, *Angew. Chem., Int. Ed.* **2010**, *49*, 1530-1532; (b) A. Betard, R. A. Fischer, *Chem. Rev.* **2012**, *112*, 1055-1083; (c) O. Shekhah, J. Liu, R. A. Fischer, C. Woll, *Chem. Soc. Rev.* **2011**, *40*, 1081-1106; (d) D. Zacher, O. Shekhah, C. Woll, R. A. Fischer, *Chem. Soc. Rev.* **2009**, *38*, 1418-1429.

[4] (a) P. Horcajada, R. Gref, T. Baati, P. K. Allan, G. Maurin, P. Couvreur, G. Férey, R. E. Morris, C. Serre, *Chem. Rev.* **2012**, *112*, 1232-1268; (b) K. M. L. Taylor, W. J. Rieter, W. B. Lin, *J. Am. Chem. Soc.* **2008**, *130*, 14358-14359.

[5] D. M. Liu, R. C. Huxford, W. B. Lin, *Angew. Chem., Int. Ed.* **2011**, *50*, 3696-3700.

[6] (a) D. Maspoch, D. Ruiz-Molina, J. Veciana, *Chem. Soc. Rev.* **2007**, *36*, 770-818; (b) D. Maspoch, D. Ruiz-Molina, K. Wurst, N. Domingo, M. Cavallini, F. Biscarini, J. Tejada, C. Rovira, J. Veciana, *Nat. Mater.* **2003**, *2*, 190-195.

[7] D. B. Dang, P. Y. Wu, C. He, Z. Xie, C. Y. Duan, *J. Am. Chem. Soc.* **2010**, *132*, 14321-14323.

[8] Z. R. Ranjbar, A. Morsali, *Inorg. Chim. Acta* **2012**, *382*, 171-176.

[9] (a) M. Bazaga-Garcia, R. M. P. Colodrero, M. Papadaki, P. Garczarek, J. Zon, P. Olivera-Pastor, E. R. Losilla, L. Leon-Reina, M. A. G. Aranda, D. Choquesillo-Lazarte, K. D. Demadis, A. Cabeza, *J. Am. Chem. Soc.* **2014**, *136*, 5731-5739; (b) M. Bazaga-Garcia, M. Papadaki, R. M. P. Colodrero, P. Olivera-Pastor, E. R. Losilla, B. Nieto-Ortega, M. A. G. Aranda, D. Choquesillo-Lazarte, A. Cabeza, K. D. Demadis, *Chem. Mater.* **2015**, *27*, 424-435; (c) R. M. P. Colodrero, K. E. Papathanasiou, N. Stavgianoudaki, P. Olivera-Pastor, E. R. Losilla, M. A. G. Aranda, L. León-Reina, J. Sanz, I. Sobrados, D. Choquesillo-Lazarte, J. M. García-Ruiz, P. Atienzar, F. Rey, K. D. Demadis, A. Cabeza, *Chem. Mater.* **2012**, *24*, 3780-3792.

[10] (a) G. K. H. Shimizu, R. Vaidhyanathan, J. M. Taylor, *Chem. Soc. Rev.* **2009**, *38*, 1430-1449; (b) P. Silva, F. Vieira, A. C. Gomes, D. Ananias, J. A. Fernandes, S. M. Bruno, R. Soares, A. A. Valente, J. Rocha, F. A. Almeida Paz, *J. Am. Chem. Soc.* **2011**, *133*, 15120-15138.

[11] L. Cunha-Silva, L. Mafra, D. Ananias, L. D. Carlos, J. Rocha, F. A. Almeida Paz, *Chem. Mater.* **2007**, *19*, 3527-3538.

[12] P. Silva, D. Ananias, S. M. Bruno, A. A. Valente, L. D. Carlos, J. Rocha, F. A. Almeida Paz, *Eur. J. Inorg. Chem.* **2013**, *2013*, 5576-5591.

[13] G. Fan, F. Li, D. G. Evans, X. Duan, *Chem. Soc. Rev.* **2014**, *43*, 7040-7066.

[14] P. Silva, F. Vieira, A. C. Gomes, D. Ananias, J. A. Fernandes, S. M. Bruno, R. Soares, A. A. Valente, J. Rocha, F. A. A. Paz, *J. Am. Chem. Soc.* **2011**, *133*, 15120-15138.

[15] J. G. Smith, *Synthesis-Stuttgart* **1984**, 629-656.

[16] (a) C. Wiles, P. Watts, S. J. Haswell, *Tetrahedron* **2005**, *61*, 5209-5217; (b) T. W. Greene, P. G. M. Wuts, in *Protective Groups in Organic Synthesis*, 3rd ed., John Wiley & Sons, Inc., Kalamazao, Michigan, **1999**, pp. 293-368; (c) D. Martin, *J. Prakt. Chem.* **1995**, *337*, 164-165.

[17] T. W. Greene, P. G. M. Wuts, *Protective Groups in Organic Synthesis*, 3 rd ed., John Wiley & Sons,, Inc., New York, USA, **1999**.

[18] (a) S. Ajaikumar, A. Pandurangan, *J. Mol. Catal. A: Chem.* **2008**, *290*, 35-43; (b) M. J. Climent, A. Velty, A. Corma, *Green Chem.* **2002**, *4*, 565-569; (c) K. Bauer, D. Garbe, H. Surburg, *Common Fragrances and Flavour Materials: Preparation and Uses, Fourth, Completely Revised Edition*, 2nd ed., Wiley-VCH Verlag GmbH, New York, USA, **2001**.

[19] (a) B. Thomas, S. Prathapan, S. Sugunan, *Microporous Mesoporous Mater.* **2005**, *80*, 65-72; (b) S. Wu, W. Dai, S. Yin, W. Li, C.-T. Au, *Catal. Lett.* **2008**, *124*, 127-132.

[20] K. Bruns, J. Conrad, A. Steigel, *Tetrahedron* **1979**, *35*, 2523-2530.

[21] A. J. Elliot, *1,3-Dioxalane Polymers in Comprehensive Heterocyclic Polymers*, Pergamon Press, Oxford, U. K., **1984**.

[22] D. M. Clode, *Chem. Rev.* **1979**, *79*, 491-513.

[23] (a) B. M. Smith, T. M. Kubczyk, A. E. Graham, *RSC Advances* **2012**, *2*, 2702-2706; (b) D. B. G. Williams, M. C. Lawton, *Green Chem.* **2008**, *10*, 914-917.

[24] D.-J. Tao, Z.-M. Li, Z. Cheng, N. Hu, X.-S. Chen, *Ind. Eng. Chem. Res.* **2012**, *51*, 16263-16269.

[25] R. F. Mendes, P. Silva, M. M. Antunes, A. A. Valente, F. A. Almeida Paz, *Chem. Commun.* **2015**, *51*, 10807-10810.

[26] S. M. F. Vilela, A. D. G. Firmino, R. F. Mendes, J. A. Fernandes, D. Ananias, A. A. Valente, H. Ott, L. D. Carlos, J. Rocha, J. P. C. Tomé, F. A. A. Paz, *Chem. Commun.* **2013**, *49*, 6400-6402.

[27] F. Vermoortele, M. Vandichel, B. Van de Voorde, R. Ameloot, M. Waroquier, V. Van Speybroeck, D. E. De Vos, *Angew. Chem., Int. Ed.* **2012**, *51*, 4887-4890.

[28] F. Vermoortele, B. Bueken, G. Le Bars, B. Van de Voorde, M. Vandichel, K. Houthoofd, A. Vimont, M. Daturi, M. Waroquier, V. Van Speybroeck, C. Kirschhock, D. E. De Vos, *J. Am. Chem. Soc.* **2013**, *135*, 11465-11468.

[29] L. H. Wee, F. Bonino, C. Lamberti, S. Bordiga, J. A. Martens, *Green Chem.* **2014**, *16*, 1351-1357.

[30] A. Herbst, A. Khutia, C. Janiak, *Inorg. Chem.* **2014**, *53*, 7319-7333.

[31] (a) A. Dhakshinamoorthy, M. Alvaro, H. Garcia, *Adv. Synth. Catal.* **2010**, *352*, 3022-3030; (b) A. Dhakshinamoorthy, M. Alvaro, P. Horcajada, E. Gibson, M. Vishnuvarthan, A. Vimont, J.-M. Grenèche, C. Serre, M. Daturi, H. Garcia, *ACS Catalysis* **2012**, *2*, 2060-2065; (c) U. S. F. Arrozi, H. W. Wijaya, A. Patah, Y. Permana, *Appl. Catal., A* **2015**, *506*, 77-84.

[32] L. Bromberg, T. A. Hatton, *ACS Appl. Mater. Interfaces* **2011**, *3*, 4756-4764.

[33] M. N. Timofeeva, V. N. Panchenko, J. W. Jun, Z. Hasan, M. M. Matrosova, S. H. Jhung, *Appl. Catal., A* **2014**, *471*, 91-97.

[34] (a) B. Thomas, V. G. Ramu, S. Gopinath, J. George, M. Kurian, G. Laurent, G. L. Drisko, S. Sugunan, *Appl. Clay Sci.* **2011**, *53*, 227-235; (b) B. Thomas, S. Sugunan, *J. Porous Mater.* **2006**, *13*, 99-106; (c) B. Thomas, S. Sugunan, *Indian J. Chem., Sect A* **2005**, *44*, 1345-1354.

[35] (a) Y. Guan, D. Zhang, Y. Wang, *Catal. Lett.* **2012**, *142*, 1225-1233; (b) J.-Y. Liu, J.-G. Wang, N. Li, H. Zhao, H.-J. Zhou, P.-C. Sun, T.-H. Chen, *Langmuir* **2012**, *28*, 8600-8607; (c) B. Rabindran Jermy, A. Pandurangan, *J. Mol. Catal. A: Chem.* **2006**, *256*, 184-192; (d) B. Thomas, S. Prathapan, S. Sugunan, *Appl. Catal., A* **2004**, *277*, 247-252.

[36] M. Iwamoto, Y. Tanaka, N. Sawamura, S. Namba, *J. Am. Chem. Soc.* **2003**, *125*, 13032-13033.

[37] C.-H. Lin, S. Lin, Y.-H. Yang, T.-P. Lin, *Catal. Lett.* **2001**, *73*, 121-125.

[38] A. Clerici, N. Pastori, O. Porta, *Tetrahedron* **1998**, *54*, 15679-15690.

[39] Y.-W. Ren, J.-X. Liang, J.-X. Lu, B.-W. Cai, D.-B. Shi, C.-r. Qi, H.-F. Jiang, J. Chen, D. Zheng, *Eur. J. Inorg. Chem.* **2011**, *2011*, 4369-4376.

[40] A. Dikhtiarenko, S. A. Khainakov, I. de Pedro, J. A. Blanco, J. R. García, J. Gimeno, *Inorg. Chem.* **2013**, *52*, 3933-3941.

[41] D. Jiang, A. Urakawa, M. Yulikov, T. Mallat, G. Jeschke, A. Baiker, *Chem.-Eur. J.* **2009**, *15*, 12255-12262.

[42] (a) P. Ramaswamy, N. E. Wong, G. K. H. Shimizu, *Chem. Soc. Rev.* **2014**, *43*, 5913-5932; (b) J. M. Taylor, R. K. Mah, I. L. Moudrakovski, C. I. Ratcliffe, R. Vaidhyanathan, G. K. H. Shimizu, *J. Am. Chem. Soc.* **2010**, *132*, 14055-14057.

[43] G. M. Sheldrick, *SHELXT-2014, Program for Crystal Structure Solution, University of Göttingen* **2014**.

[44] (a) G. M. Sheldrick, *Acta Cryst. A* **2008**, *64*, 112-122; (b) G. M. Sheldrick, *SHELXL Version 2014, Program for Crystal Structure Refinement, University of Göttingen* **2014**.

[45] C. B. Hübschle, G. M. Sheldrick, B. Dittric, *J. Appl. Crystallogr.* **2011**, *44*, 1281-1284.

[46] K. Brandenburg, *DIAMOND, Version 4.0.0. Crystal Impact GbR, Bonn, Germany* **1997-2014**.

Table 1. Crystal data collection and structure refinement details for $[Gd(H_4nmp)(H_2O)_2]Cl{\cdot}2H_2O$ (**1**).

Formula	$C_3H_{18}ClGdNO_{13}P_3$
Formula weight	561.79
Temperature / K	160(2)
Crystal system	Monoclinic
Space group	*I*a
a / Å	8.53794(13)
b / Å	17.4871(3)
c / Å	10.76816(18)
β / º	110.6216(18)
Volume / Å^3	1504.71(5)
Z	4
ρ_{calc}/ g cm^{-3}	2.480
*m(*Mo K*a)* / mm^{-1}	4.970
Crystal type	Colourless plate
Crystal size / mm	0.05×0.25×0.27
θ range (°)	3.519–29.130
Index ranges	$-11 \le h \le 11$
	$-23 \le k \le 23$
	$-14 \le l \le 14$
Collected Reflections	10433
Independent Reflections	4003 (R_{int} = 0.0265)
Completeness to θ=27.48	99.8%
Final *R* indices [$I>2\sigma(I)$][a-c]	$R1$ = 0.0185
	$wR2$ = 0.0387
Final *R* indices (all data)[a-c]	$R1$ = 0.0202
	$wR2$ = 0.0396
Absolute Structure Parameter	-0.012(5)
Largest diff. peak and hole /eÅ^{-3}	0.666 and -0.869

[a] $R1 = \sum \| |F_o| - |F_c| \| / \sum |F_o|$

[b] $wR2 = \sqrt{\sum \left[w\left(F_o^2 - F_c^2\right)^2 \right] / \sum \left[w\left(F_o^2\right)^2 \right]}$

[c] $w = 1/\left[\sigma^2\left(F_o^2\right) + \left(mP\right)^2 + nP \right]$ where $P = \left(F_o^2 + 2F_c^2\right)/3$

Table 2. Selected bond lengths (in Å) and angles (in degrees) for the Gd^{3+} crystallographically independent coordination environment present in $[Gd(H_4nmp)(H_2O)_2]Cl{\cdot}2H_2O$ (**1**).[a]

Gd1–O1	2.371(3)	Gd1–O7^{ii}	2.338(3)
Gd1–O2^{iii}	2.354(3)	Gd1–O8^{i}	2.326(3)
Gd1–O5^{iii}	2.396(3)	Gd1–O1W	2.564(3)
Gd1–O6	2.382(3)	Gd1–O2W	2.434(3)
O1–Gd1–O5^{iii}	124.50(11)	O7^{ii}–Gd1–O1	79.23(12)
O1–Gd1–O6	75.43(11)	O7^{ii}–Gd1–O2^{iii}	150.53(11)
O1–Gd1–O1W	126.67(11)	O7^{ii}–Gd1–O5^{iii}	135.64(12)
O1–Gd1–O2W	68.54(12)	O7^{ii}–Gd1–O6	81.61(11)
O2^{iii}–Gd1–O1	79.51(11)	O7^{ii}–Gd1–O1W	65.37(11)
O2^{iii}–Gd1–O5^{iii}	73.69(11)	O7^{ii}–Gd1–O2W	86.06(13)
O2^{iii}–Gd1–O6	73.45(11)	O8^{i}–Gd1–O1	149.58(12)
O2^{iii}–Gd1–O1W	144.01(11)	O8^{i}–Gd1–O2^{iii}	94.94(12)
O2^{iii}–Gd1–O2W	104.74(13)	O8^{i}–Gd1–O5^{iii}	81.20(11)
O5^{iii}–Gd1–O1W	70.86(11)	O8^{i}–Gd1–O6	74.32(12)
O5^{iii}–Gd1–O2W	72.68(12)	O8^{i}–Gd1–O7^{ii}	93.16(12)
O6–Gd1–O5^{iii}	136.67(11)	O8^{i}–Gd1–O1W	73.81(12)
O6–Gd1–O1W	131.97(11)	O8^{i}–Gd1–O2W	140.89(12)
O6–Gd1–O2W	143.49(12)	O2W–Gd1–O1W	70.41(13)

[a] Symmetry transformations used to generate equivalent atoms: (i) $x+1,y,z$; (ii) $x+1,-y+1/2, z+1/2$;(iii) $x,-y+1/2,z-1/2$;(iv) $x ,-y+1/2,z+1/2$.

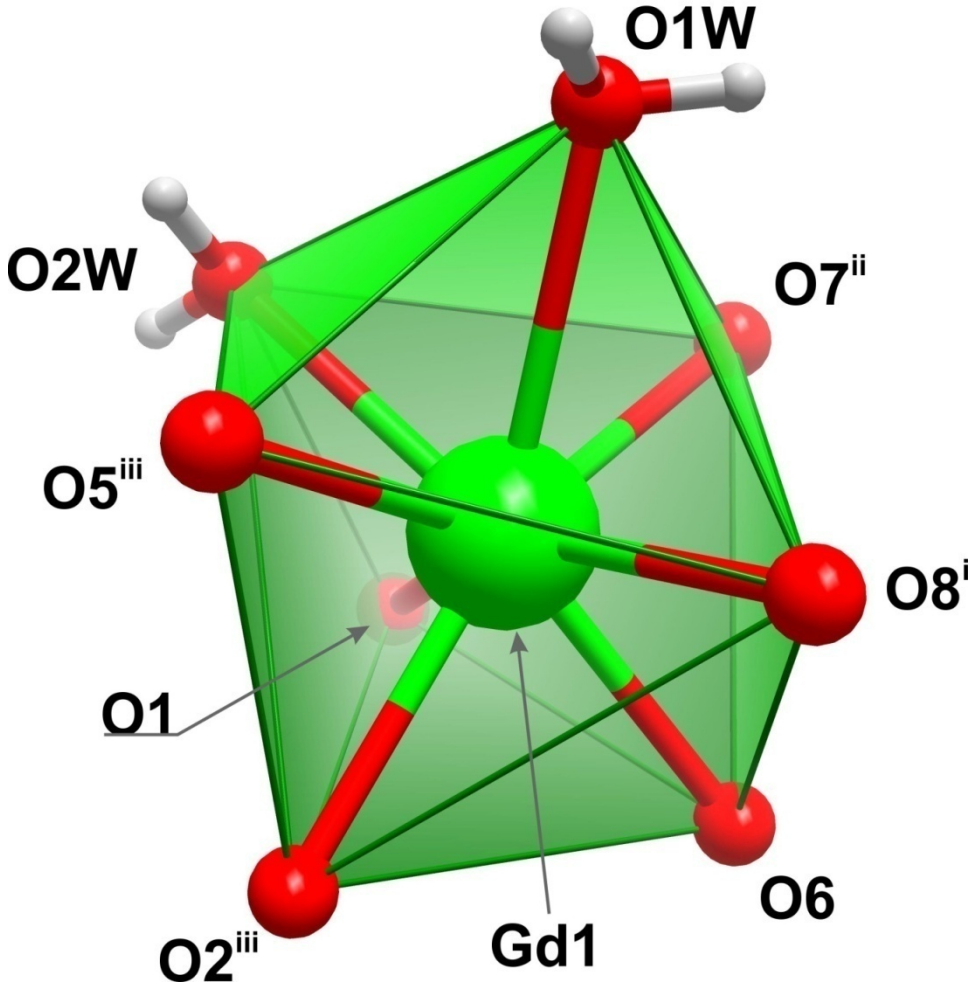

Figure 1. Polyhedral representation of the distorted $\{GdO_8\}$ dodecahedral coordination environment present in compound $[Gd(H_4nmp)(H_2O)_2]Cl{\cdot}2H_2O$ (**1**). Symmetry transformations used to generate equivalent atoms: (i) *x*+1,*y*,*z*;(ii) *x*+1,-*y*+1/2, *z*+1/2;(iii) *x*,-*y*+1/2,*z*-1/2.

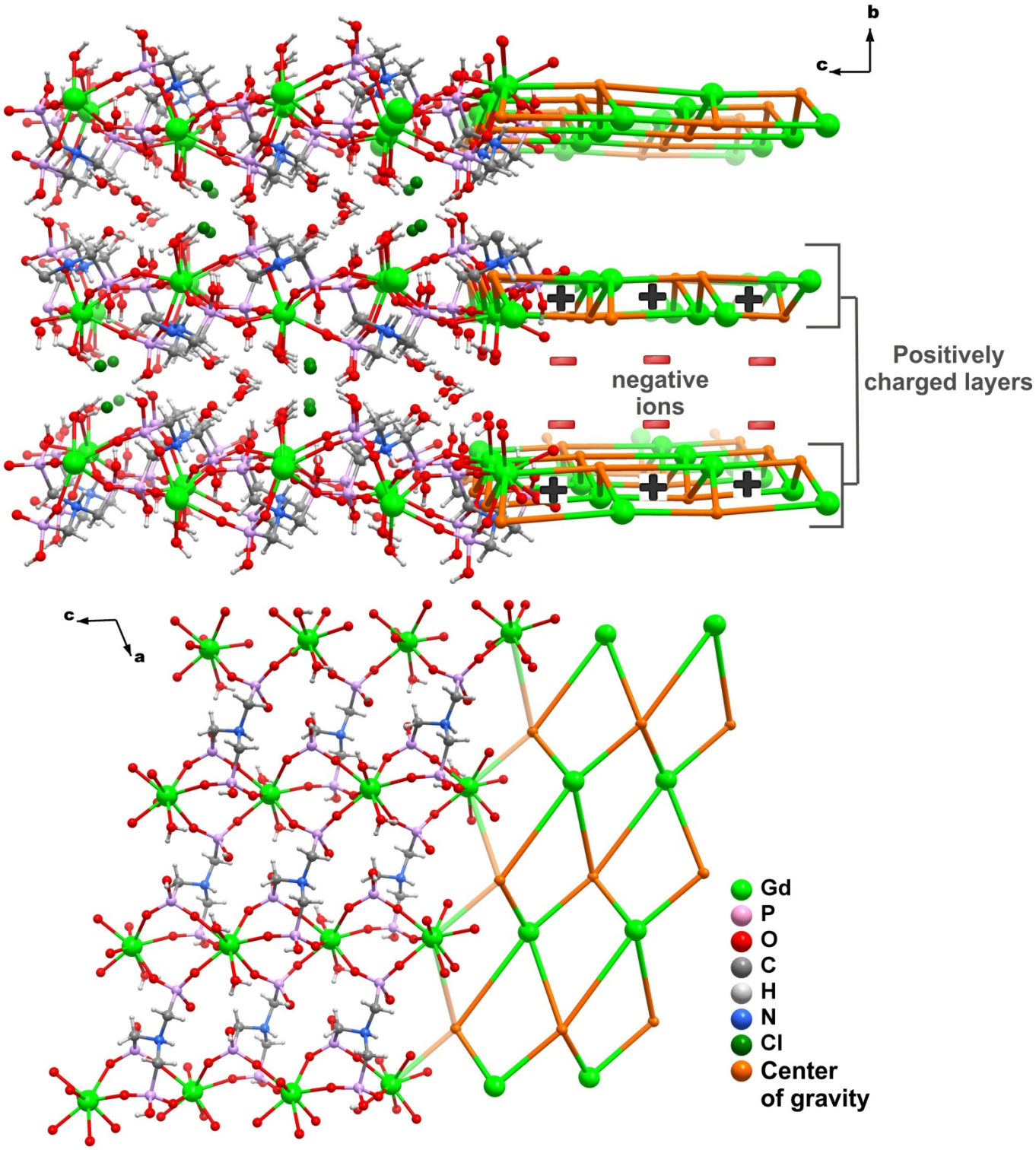

Figure 2. Schematic representation of the (*top*) crystal packing of $[Gd(H_4nmp)(H_2O)_2]Cl{\cdot}2H_2O$ (**1**) viewed in perspective along the [100] direction of the unit cell, and of the (*bottom*) $_\infty^2[Gd(H_4nmp)(H_2O)_2]^+$ cationic layer. The 4-connected uninodal topology of the cationic layers is overlapped in both representations.

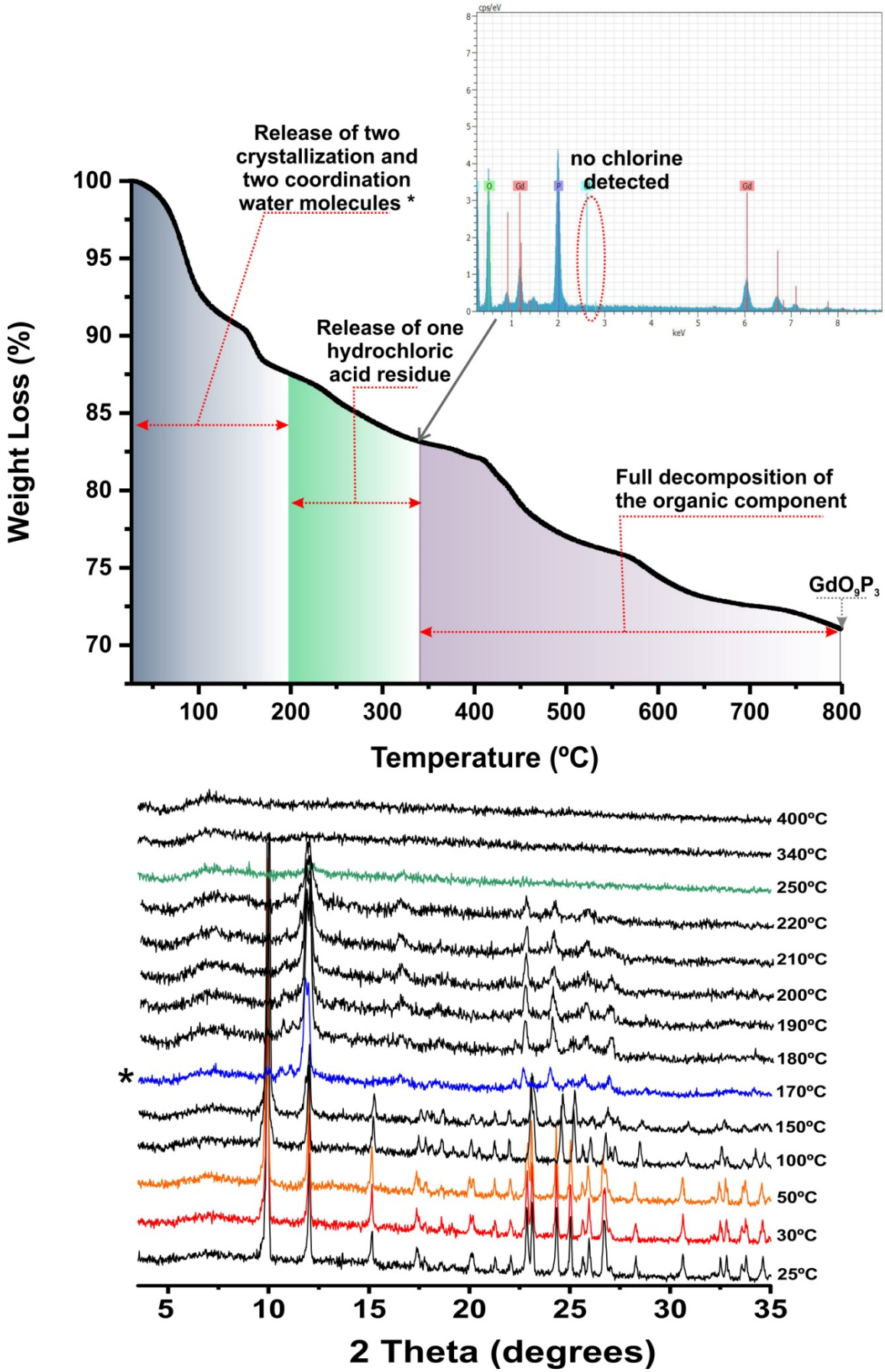

Figure 3. Themogram and thermodiffractometry studies of $[Gd(H_4nmp)(H_2O)_2]Cl{\cdot}2H_2O$ (**1**) between ambient temperature and*ca.* 800 ºC. EDS analyses show theabsence of chlorine atoms in the sample calcined at 350 ºC.

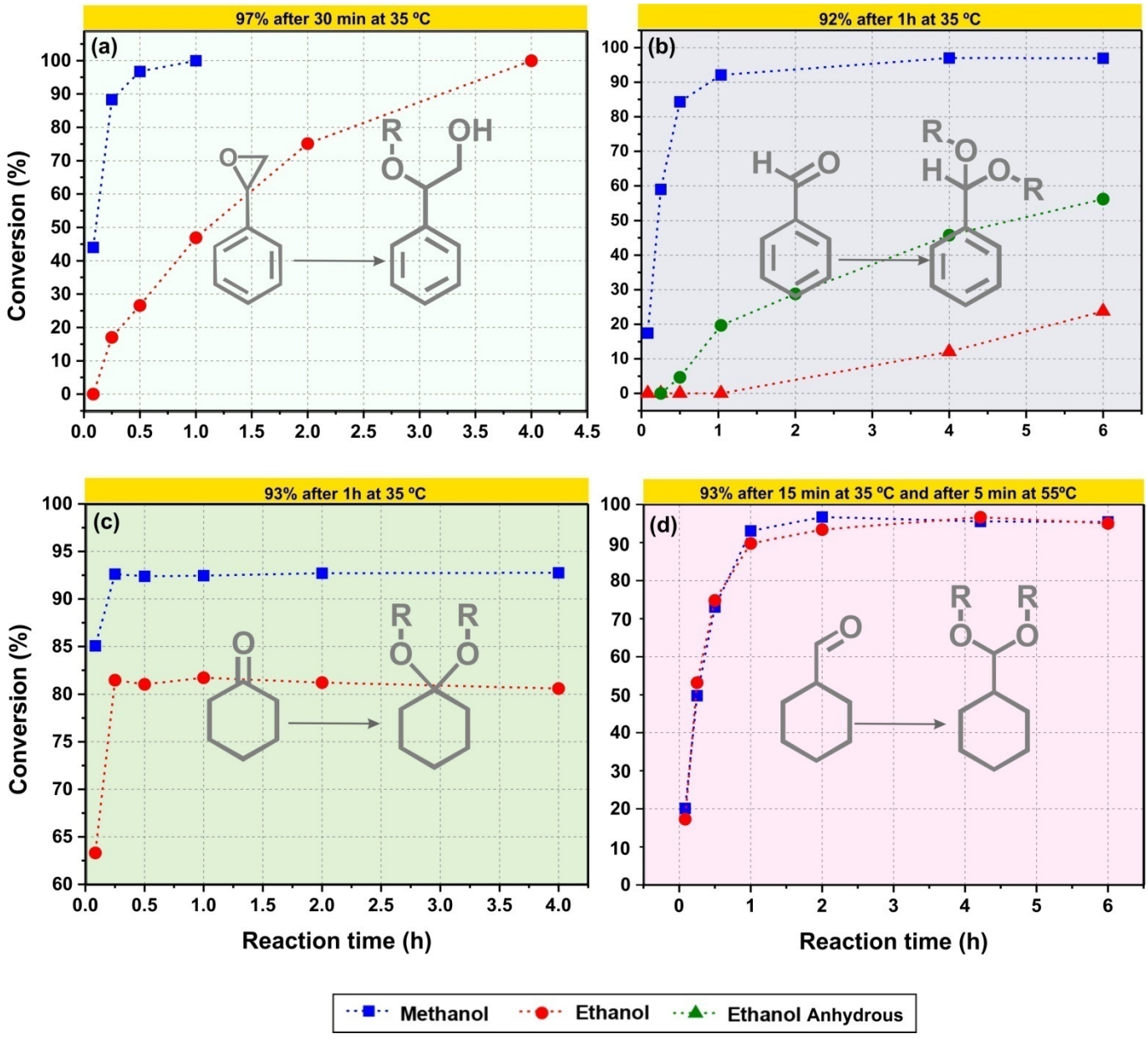

Figure 4. Conversion of **(a)** styrene oxide, **(b)** benzaldehyde, **(c)** cyclohexanone and **(d)** cyclohexaldehyde with methanol or ethanol, in the presence of $[Gd(H_4nmp)(H_2O)_2]Cl{\cdot}2H_2O$ (**1**) (catalyst load=$20 g_1\ L^{-1}$). *Please note*: dashed lines connecting experimental points are only for illustrative purposes. R = CH_3 or CH_2CH_3.

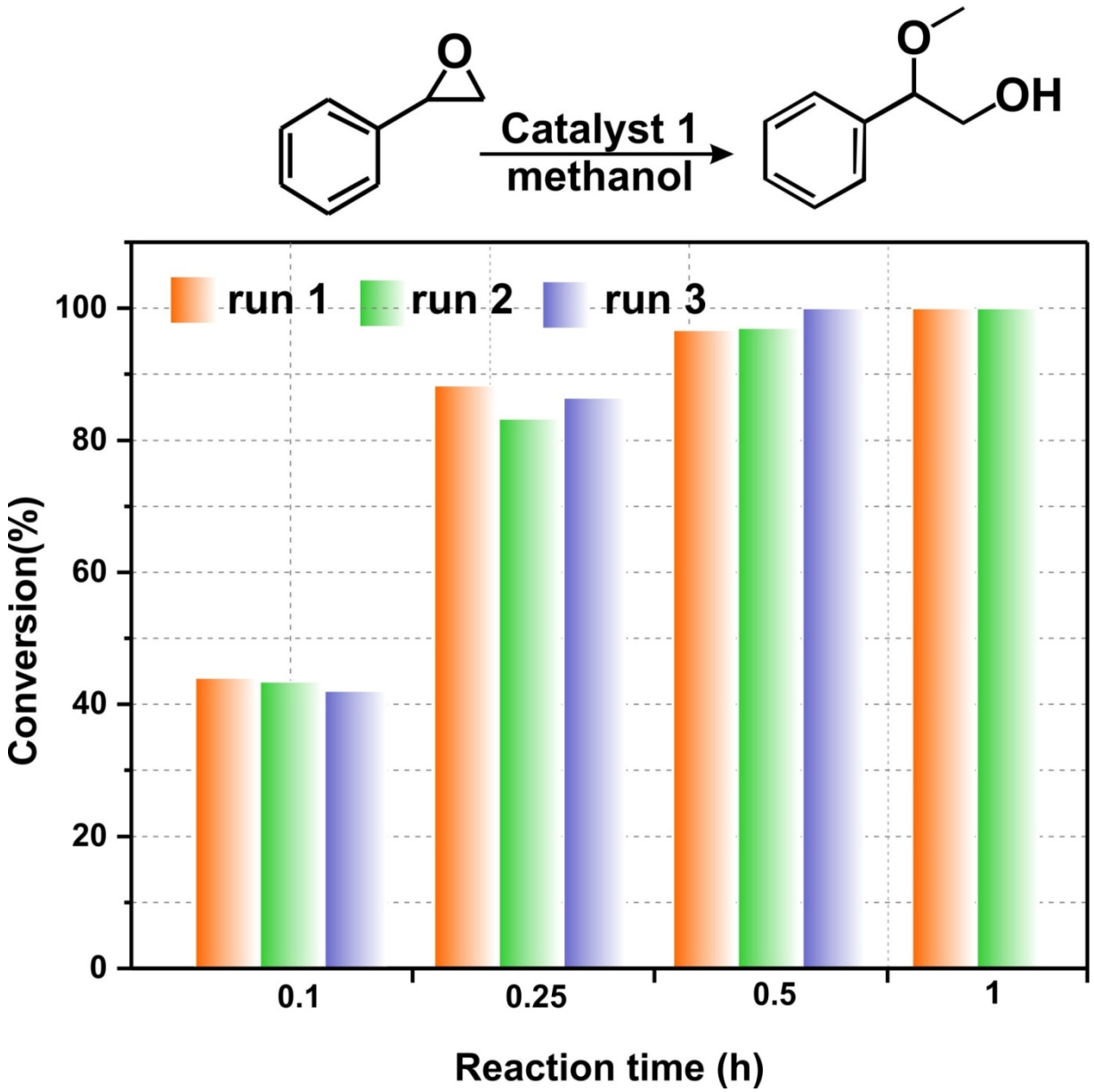

Figure 5. Conversion of styrene oxide in methanol in the presence of $[Gd(H_4nmp)(H_2O)_2]Cl{\cdot}2H_2O$ (**1**) at 35 ºC (catalyst load = 20 g^1 L^{-1})used in three consecutive batch runs of the methanolysis of styrene oxide.

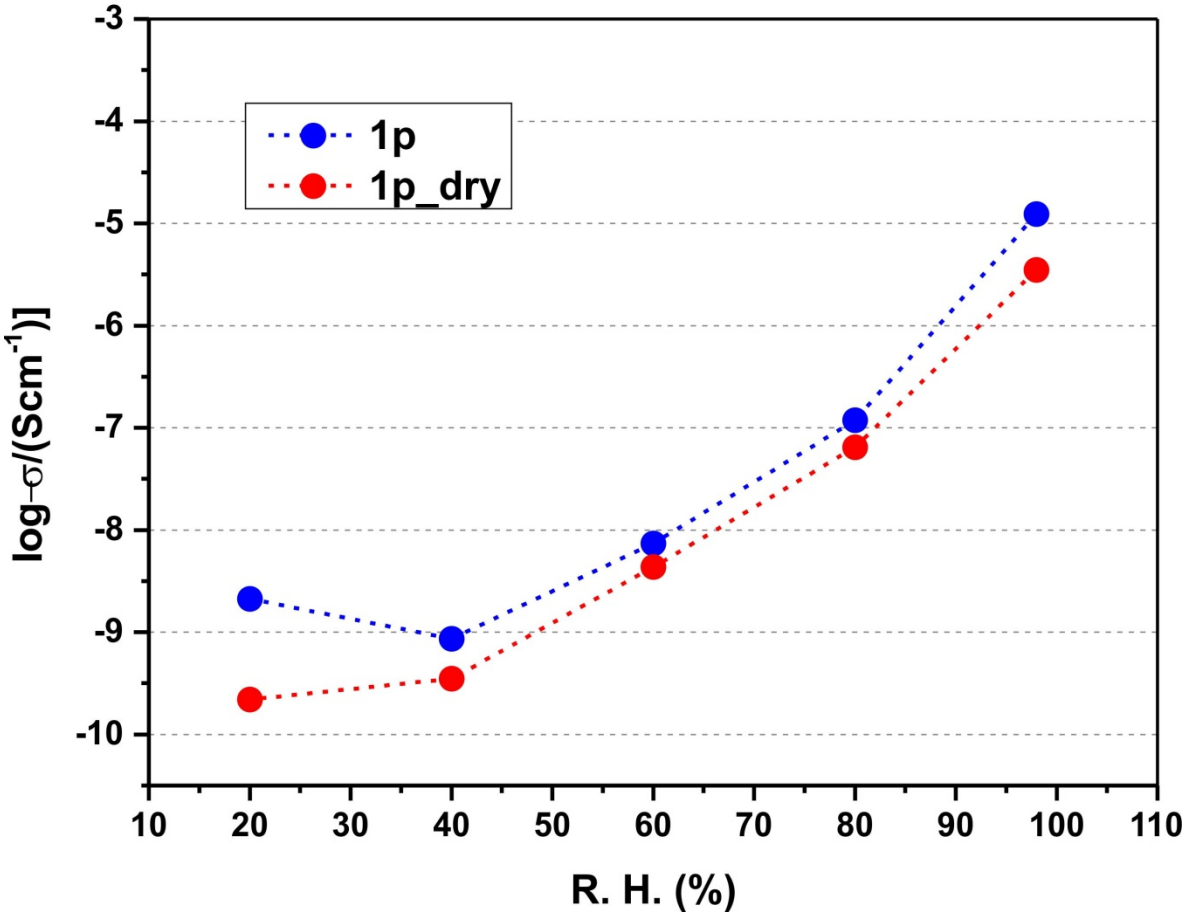

Figure 6. Protonic conductivity at 40 °C as a function of RH for **1p** and **1p_dry**.